HHS Public Access

Author manuscript

Bone. Author manuscript; available in PMC 2024 November 01.

Published in final edited form as:

Bone. 2023 November ; 176: 116886. doi:10.1016/j.bone.2023.116886.

Contributions of increased osteopontin and hypophosphatemia to dentoalveolar defects in osteomalacic *Hyp* mice

Fatma F Mohamed[1], **Betty Hoac**[2], **Aonjittra Phanrungsuwan**[1], **Michelle H. Tan**[1], **Priscila Alves Giovani**[3], **Sana Ghiba**[1], **Monzur Murshed**[2,5,6], **Brian L Foster**[1], **Marc D McKee**[2,4]

[1] Division of Biosciences, College of Dentistry, The Ohio State University, Columbus, OH, USA

[2] Faculty of Dental Medicine and Oral Health Sciences, McGill University, Montreal, QC, Canada

[3] Campinas State University, School of Dentistry, Piracicaba, São Paulo, Brazil

[4] Department of Anatomy and Cell Biology, School of Biomedical Sciences, Faculty of Medicine and Health Sciences, McGill University, Montreal, QC, Canada

[5] Department of Medicine, Faculty of Medicine, McGill University, Montreal, QC, Canada

[6] Shriners Hospital for Children, Montreal, QC, Canada

Abstract

X-linked hypophosphatemia (XLH) is an inherited disorder caused by inactivating mutations in the *PHEX* gene leading to renal phosphate wasting, rickets and osteomalacia. XLH is also associated with dentoalveolar mineralization defects in tooth enamel, dentin and cementum, and in alveolar bone, which lead to an increased prevalence of dental abscesses, periodontal disease and tooth loss. Genetic mouse experiments, and deficiencies in XLH patient therapies where treatments do not fully ameliorate mineralization defects, suggest that other pathogenic mechanisms may exist in XLH. The mineralization-inhibiting, secreted extracellular matrix phosphoprotein osteopontin (OPN, gene *Spp1*) is a substrate for the PHEX enzyme whereby extensive and inactivating degradation of inhibitory OPN by PHEX facilitates mineralization. Conversely, excess OPN

Co-corresponding authors: Brian L. Foster, PhD, Biosciences Division, College of Dentistry, The Ohio State University, 4163 Postle Hall, 305 W. 12th Avenue, Columbus, OH 43210, USA, foster.1004@osu.edu, Marc D. McKee, PhD, Dental Medicine and Oral Health Sciences, McGill University, 3640 University Street, Montreal, QC, Canada, H3A 0C7, marc.mckee@mcgill.ca.

Declaration of competing interest

The authors declare no conflict of interest.

CRediT authorship contribution statement

Fatma F. Mohamed: Conceptualization, Formal analysis, Investigation, Methodology, Visualization, Writing – original draft. **Betty Hoac:** Conceptualization, Formal analysis, Investigation, Methodology, Visualization, Writing – review & editing. **Aonjittra Phanrungsuwan:** Investigation, Methodology, Writing – original draft. **Michelle Tan:** Investigation, Methodology**. Priscila Alves Giovani:** Investigation, Methodology. **Sana Ghiba:** Investigation, Methodology **Monzur Murshed:** Conceptualization, Writing – review & editing. **Marc D. McKee:** Conceptualization, Formal analysis, Funding Acquisition, Investigation, Methodology, Project administration, Supervision, Visualization, Writing – original draft. **Brian L. Foster:** Conceptualization, Formal analysis, Funding Acquisition, Investigation, Methodology, Project administration, Supervision, Visualization, Writing – original draft.

Appendix A.

Supplementary data to this article include three figures.

accumulation in skeletal and dental tissues – for example in XLH where inactivating mutations in the *PHEX* gene limit degradation of inhibitory OPN, or as occurs in *Fgf23*-null mice – contributes to mineralization defects. We hypothesized that *Spp1*/OPN ablation in *Hyp* mice (a mouse model for XLH) would reduce dentoalveolar mineralization defects. Immunostaining revealed increased OPN in *Hyp* vs. wild-type (WT) alveolar bone, particularly in osteocyte lacunocanalicular networks where *Hyp* mice have characteristic hypomineralized peri-osteocytic lesions (POLs). Micro-computed tomography and histology showed that ablation of *Spp1* in *Hyp* mice (*Hyp;Spp1*$^{-/-}$) on a normal diet did not ameliorate bulk defects in enamel, dentin, or alveolar bone. On a high-phosphate diet, both *Hyp* and *Hyp;Spp1*$^{-/-}$ mice showed improved mineralization of enamel, dentin, and alveolar bone. Silver staining indicated *Spp1* ablation did not improve alveolar or mandibular bone osteocyte POLs in *Hyp* mice; however, they were normalized by a high-phosphate diet in both *Hyp* and *Hyp;Spp1*$^{-/-}$ mice, although inducing increased OPN. Collectively, these data indicate that despite changes in OPN content in the dentoalveolar mineralized tissues, there exist other compensatory mineralization mechanisms that arise from knockout of *Spp1*/OPN in the *Hyp* background.

Keywords

X-linked hypophosphatemia; osteomalacia; bone; teeth; osteopontin; periodontium

1. Introduction

X-linked hypophosphatemia (XLH; OMIM:307800) is the most common form of hereditary rickets and osteomalacia at ~1:20,000 births [1]. XLH is caused by inactivating mutations in the gene for the enzyme PHEX (*PHEX*, phosphate-regulating endopeptidase homolog X-linked) [2]. *PHEX* mutations lead to hypomineralization causing soft bones and teeth that easily deform, bend and fracture. Through mechanisms that remain incompletely understood, *PHEX* mutations lead to increased fibroblast growth factor 23 (FGF23) levels, decreased vitamin D ($1,25(OH)_2D_3$) levels, and increased excretion of inorganic phosphate (P_i) causing hypophosphatemia. Skeletal manifestations of XLH include rachitic bowing of long bones, osteomalacia, and growth plate defects. XLH is associated with severe dentoalveolar mineralization defects [3–5]. Defects in enamel and dentin (odontomalacia) contribute to a high prevalence of dental abscesses, while cementum and alveolar bone mineralization defects are associated with increased prevalence of periodontal disease – these contribute to early tooth loss, lifelong disease burden, and decreased oral and overall health.

Conventional treatment for XLH includes oral P_i and $1,25(OH)_2D_3$ supplements; these only partially ameliorate skeletal and dentoalveolar mineralization defects [6]. An FGF23-targeting monoclonal antibody (burosumab; Crysvita®) was approved in 2018 (USA, and elsewhere) for treatment of adult and pediatric XLH patients [7, 8]. Burosumab improves mineral ion metabolism and skeletal manifestations of XLH; however, effects on dentoalveolar tissues remain unclear due in part to conflicting reports of increased or decreased prevalence of dental abscesses or caries [9–12]. *Hyp* mice carrying loss-of-function mutations in *Phex* replicate key aspects of the skeletal and dental phenotypes

observed in human XLH [5, 13]. A study in *Hyp* mice comparing $1,25(OH)_2D_3$ to FGF23-neutralizing antibody (FGF23Ab) showed that neither treatment fully attenuated dentoalveolar defects, although $1,25(OH)_2D_3$ promoted more profound improvements in dentin, cementum, and alveolar bone [14]. The inability of either treatment to fully correct XLH-associated dentoalveolar defects suggests that there exist other pathogenic mechanisms that are not addressed by current therapeutic approaches.

The extracellular matrix (ECM) protein osteopontin (OPN) regulates and inhibits mineralization *in vitro* and *in vivo* [15, 16]. Genetic deletion of *Spp1*/OPN in mice supports a role in regulating dentin and alveolar bone formation and mineralization [17]. PHEX, expressed by osteoblasts, osteocytes, odontoblasts, and cementocytes, extensively cleaves and inactivates the mineralization-regulating properties of OPN [18–20]. Increased OPN in bones and teeth in XLH is implicated in XLH-associated mineralization defects and is not addressed by conventional therapy or FGF23Ab [21–24]. Genetic ablation of *Spp1*/OPN in *Hyp* mice improved mineralization in tibias and vertebrae independent of systemic mineral metabolism [25]. In the present study, we hypothesized that *Spp1*/OPN ablation in *Hyp* mice would reduce XLH/*Hyp*-associated dentoalveolar defects. We used a multimodal approach to analyze the effects of *Spp1* ablation on the *Hyp* background on enamel, dentin, cementum, and alveolar bone after mice were fed either a normal or high-phosphate diet.

2. Materials and methods

2.1. Mice

Double-null *Hyp;Spp1*$^{-/-}$ mice were generated and genotyped as previously described in [25]. *Spp1*$^{-/-}$ mice and *Hyp* mice (B6.Cg-*Phex*^{Hyp}/J) on the C57BL/6 background were obtained from the Jackson Laboratory (Bar Harbor, ME, USA). Mice were fed *ad libitum* with normal mouse chow, referred to as the control (CTR) diet (2090X Teklad global soy protein-free extruded rodent diet modified to 1.1% calcium and 0.7% phosphate, Envigo, Huntingdon, UK), or with a high-phosphate (HP) diet (2090X modified to 1.1% calcium and 2.0% phosphate), administered once weaned at 3 weeks old for 4 consecutive weeks with water supplied also *ad libitum* [25]. Mice were euthanized and tissues were harvested at 50 days postnatal (dpn). All animal procedures were reviewed and approved by the McGill University Institutional Animal Care and Use Committee, and they followed the guidelines of the Canadian Council on Animal Care.

2.2. Micro-computed tomography (micro-CT)

Right hemi-mandibles (n=3) fixed in 0.1% glutaraldehyde plus 4.0% paraformaldehyde in 0.1 M sodium cacodylate buffer pH 7.3 were scanned in a μCT 50 (Scanco Medical, Bassersdorf, Switzerland) at 70 kVp, 76 μA, 0.5 mm Al filter, 900 ms integration time, and 6 μm voxel size. DICOM files were reconstructed, calibrated to five known densities of hydroxyapatite (mg/cm^3 HA) and analyzed using Analyze 14 software (AnalyzeDirect, Overland Park, KS, USA) as previously described [26, 27]. Briefly, hemi-mandibles were oriented using first molar (M1) anatomical landmarks and micro-CT analysis was performed using a region of interest (ROI) including M1 molar and surrounding alveolar bone (240 μm mesial to the mesial root to 240 μm distal to the distal root, including buccal and lingual

aspects of alveolar bone). Enamel was segmented at >1,600 mg/cm^3 HA. Dentin/cementum and bone were segmented at >450 mg/cm^3 HA [26]. For cellular cementum analysis, a mask was created by applying a median filter using a kernel size of 11 and then segmenting cellular cementum between 450–1050 mg/cm^3 HA. Manual correction was performed to exclude dentin. The segmented mask was loaded onto the original calibrated volume to segment cellular cementum underneath the mask at a density >650 mg/cm^3 HA.

2.3. Histology

Left hemi-mandibles were processed for histology after fixation for 1 h at room temperature, and then overnight, in combined 0.1% glutaraldehyde plus 4.0% paraformaldehyde in 0.1 M sodium cacodylate buffer pH 7.3, followed by rinsing and storage 0.1 M sodium cacodylate buffer pH 7.3. Decalcification was performed in a solution of 10% v/v glacial acetic acid, 0.4% v/v neutral buffered formalin, and 0.85% w/v sodium chloride (AFS) solution under agitation for 4–5 weeks at 4°C, and paraffin embedding and sectioning (6-μm serial sectioning) was performed [28]. Glass slide-mounted histology sections were deparaffinized in xylene and rehydrated in an ethanol series. Deparaffinized sections were stained by hematoxylin and eosin (H&E), toluidine blue (TB), and picrosirius red (PR) as previously described [28]. Tartrate-resistant acid phosphatase (TRAP) staining was performed according to manufacturer's instructions to identify osteoclasts [29]. Immunohistochemistry (IHC) was performed using an avidin-biotinylated peroxidase-based kit with a 3-amino-9-ethylcarbazole substrate (Vector Labs, Burlingame, CA, USA) to produce a red-brown product (n=3 mice/genotype). IHC was performed on deparaffinized sections with polyclonal rabbit anti-mouse osteopontin (OPN) IgG (LF-175; Dr Larry Fisher, NIDCR, Bethesda, MD, USA) [17, 30, 31].

2.4. Histomorphometry

Histomorphometry was performed on representative sections from the n=3 mice/experimental group. For predentin thickness, H&E-stained tissue sections were measured at 40X magnification using Analyze 14.0 software. Predentin thickness was measured using the middle one-third of the mesial root as a region of interest (ROI). Predentin area was segmented using a range of 100–400 threshold values of the red channel and manually correcting to capture only predentin area. Thickness was then calculated by dividing predentin area over the length of segmented area. For acellular and cellular cementum, measurements were made using ImageJ version 1.52q (National Institutes of Health, Bethesda, MD, USA). Thicknesses of acellular cementum were measured at 90, 100, and 110 μm apical to the cementum-enamel junction (CEJ) on the buccal side of first molar in coronal sections of the mesial root at 40X magnification. Thickness values were then averaged for each sample. In *Hyp* mice on the CTR diet, cellular cementum was not reliably detectable by micro-CT due to the accumulation of cementoid (unmineralized cementum) and segmentation of cellular cementum from dentin was not possible due to severe mineralization defects in both tissues. In order to quantify effects of genotype and diet on cementum, cellular cementum was analyzed using H&E stained images, where the cellular cementum (CC) area was measured at 5X magnification in coronal sections of the mesial root, combining buccal and lingual cellular cementum area measurements to a total cellular cementum area.

To determine the cementoid-to-cementum ratio, a representative histological image for each sample was processed twice. First, H&E-stained images captured at 20X magnification were converted to 8-bit grayscale, brightness and contrast were automatically enhanced, and a 16-color color map was applied to 8-bit grayscale images to reflect the range of grey value intensities in colors, with red color representing the lowest intensity and dark blue color representing the highest intensity. Images in 16-colors were used as maps to define low intensity (red color) regions as cementoid, while remaining regions were defined as “mineralized” cementum. To measure the cementoid-to-cementum ratio, the brightness and contrast of H&E-stained images were enhanced to clearly define cellular cementum from mantle dentin (the thin outermost dentin layer). The images were traced using the freehand selection tool in ImageJ to exclude mantle dentin and other tooth structures in order to capture only cellular cementum. H&E-traced images showing only cellular cementum were converted to 8-bit greyscale images. As human eyes cannot accurately distinguish the range of grey value intensities in the greyscale images, the color-mapped images were used as a guide to apply threshold using red color on the greyscale images. The “mineralized” cementum area was segmented between 60 to 200 threshold values, whereas the total area was defined between 60–255 threshold values. Cementoid area was calculated by subtracting “mineralized” cementum area from the total area, while the cementoid-to-cementum ratio was calculated by dividing cementoid area by “mineralized” cementum.

2.5. Ploton silver staining

To analyze osteocyte and cementocyte lacunocanalicular networks, Ploton silver staining of coronal mandible sections was performed as previously described [26]. Briefly, 6-μm-thick deparaffinized sections were incubated with freshly prepared 50% silver nitrate (Fisher Scientific, catalog# BP2546–100) in gelatin-formic acid solution in the dark for 55 minutes at room temperature. Silver-stained sections were incubated for 10 minutes in 5% sodium thiosulfate (Fisher Scientific, Waltham, MA, USA) and then counterstained with 0.1% Cresyl violet solution (Acros Organics, Geel, Belgium) for 5 minutes to stain cell nuclei. Stained sections were dehydrated and coverslipped. Silver-stained images were captured using a 63X objective lens on a light microscope (Nikon E600) and analyzed using FiJi/imageJ (version 2.0.0- rc-69/1.52p; https://imagej.nih.gov/ij/). Genotypes of study groups were not identified during analysis to avoid bias.

For quantification of osteocyte parameters, we used alveolar and mandibular basal bones (n=3 mice/experimental group). Alveolar bone regions included buccal bone, while basal bone included bone of the inferior cortical plate not associated with molar attachment. Osteocyte density was defined by the number of osteocytes normalized to the total bone area in each image captured. Total bone area (whole area) was traced using the freehand selection function in FiJi/ImageJ. Because the osteocyte density was reduced in *Hyp* samples, ten silver-stained lacunae containing single Cresyl violet-stained cells were selected to quantify lacunar and canalicular parameters and detect any differences among the groups. To measure lacunar area and major and minor axes (height and width, respectively) of osteocytes in alveolar bone, the perimeter of each lacuna was traced using the freehand selections function in FiJi/ImageJ. For analysis of osteocyte canaliculi in alveolar bone, the number of canaliculi per osteocyte and length of canalicular projections were manually traced from ten osteocytes

using the freehand line function in FiJi/ImageJ. For cellular cementum, all cementocyte lacunae fully surrounded by cementum were analyzed on buccal and lingual aspects of the apical molar root. Cells on the tooth dentin surface and at the edge of cementum were not included in the analysis because some of these are remnants of Hertwig's epithelial root sheath (HERS). The resulting number of lacunae was normalized to the total cellular cementum area for each sample. Silver-stained cementocytes did not show clearly defined canaliculi, therefore, only lacunar area (measurement of all cementocyte lacunar areas divided by the number of cementocytes), height, and width per cementocyte were analyzed using the freehand selections function in FiJi/ImageJ.

2.6. Statistical Analysis

Sample size for each analysis was calculated using a one-way analysis of variance (ANOVA) power analysis assuming an alpha error of 0.05, a power of 0.9, and an estimated effect size appropriate for each analysis [25]. Statistical analysis of data was performed using either two-way ANOVA (to compare genotype and diet effects and their interaction) or one-way ANOVA (to compare genotype effects for measurements not done across diet), followed by post-hoc Tukey test (Prism version 9.1; GraphPad Software), with α=0.05. Data for all experimental groups are presented as mean ± standard deviation (SD). Statistical significance is indicated by: * P<0.05; ** P<0.01; *** P<0.001; **** P<0.0001. Inclusion of no marker for statistical significance means P>0.05.

3. Results

3.1. Spp1 (OPN) ablation in Hyp mice does not rescue most dentoalveolar mineralization defects

Loss-of-function *Phex* mutations in *Hyp* mice lead to hypophosphatemia and mineralization defects in the skeleton as well as in dentoalveolar tissues, including enamel, dentin, cementum and bone [3, 13, 22]. Immunohistochemistry showed increased and altered localization of OPN in *Hyp* vs. WT dentoalveolar tissues, particularly in alveolar bone and cellular cementum (Fig. 1A–D). As reported previously, genetic ablation of *Spp1*/OPN partially rescued tibial and lumbar vertebrae mineralization in *Hyp* mice, though *Hyp;Spp1*$^{-/-}$ double-deficient mice remained hypophosphatemic [25]. In the present study, we aimed to determine whether OPN contributes to dentoalveolar mineralization defects in *Hyp* mice by comparing *Hyp;Spp1*$^{-/-}$ double-deficient mice to controls.

Micro-CT analysis of the first mandibular molar (M1) and associated alveolar bone showed no substantial differences in tooth tissue volumes or densities between WT and *Spp1*$^{-/-}$ mice at 50 dpn (Fig. 1E–I). Decreased dentin/cementum volume (25–30%) and dentin/cementum density (7%) in *Hyp* vs. WT mice were not ameliorated in *Hyp;Spp1*$^{-/-}$ mice. Dentin and cementum could not be reliably segmented and analyzed separately in *Hyp* or *Hyp;Spp1*$^{-/-}$ mice due to the severe mineralization defects in both tissues. *Hyp;Spp1*$^{-/-}$ molars showed a small but statistically significant (7%) reduction in pulp volume compared with *Hyp* mice, though values were still more than twice those of WT mice. Significantly decreased bone volume fraction (BV/TV; 23–27%) and bone mineral density (BMD; 22–23%) remained unimproved in *Hyp;Spp1*$^{-/-}$ vs. *Hyp* mice. Increased periodontal ligament

(PDL) volume in *Hyp* vs. WT mice (24–32%) was similarly unaltered by OPN knockout in *Hyp;Spp1*$^{-/-}$ mice.

Histology showed normal tissue organization of dentoalveolar tissues in *Spp1*$^{-/-}$ and WT mice, while both *Hyp* and *Hyp;Spp1*$^{-/-}$ mice exhibited thin dentin with hypomineralized interglobular patterns, widened predentin, cementoid and osteoid accumulation, and compromised PDL attachment to alveolar bone (Fig. 2A–C). No differences were found in acellular cementum thickness among experimental groups (Fig. 2E). Increased predentin thickness (83–91%) in *Hyp* mice was not improved in *Hyp;Spp1*$^{-/-}$ mice. H&E and TB staining (Supplemental Fig. S1A) indicate unmineralized vs. mineralized regions in the tissue based on staining intensity (mineralized regions stain more darkly because of the accumulation of noncollagenous mineral-binding proteins at these sites) – *e.g.* predentin vs. dentin, osteoid vs. bone, and cementoid vs. cementum – and mineralization defects are severe enough to allow estimated quantification of the extent of mineralization based on this staining appearance [4, 13]. Using an ImageJ color map quantification based on H&E stain intensities, *Hyp* mice exhibited higher cementoid/cementum ratio, supporting defective mineralization in cellular cementum compared with WT and *Spp1*$^{-/-}$ mice (Fig. 2D, E). *Hyp;Spp1*$^{-/-}$ molars showed significantly reduced cementoid/cementum ratio (48%) compared to *Hyp* mice.

3.2. Lack of improvement of the bone lacunocanalicular system after deletion of Spp1 (OPN) in Hyp mice

Hyp mouse craniofacial and postcranial bones show altered cell densities and lacunocanalicular properties of osteocytes, with hypomineralized peri-osteocytic lesions (POLs, halos) and canaliculi showing increased OPN localization (see Fig. 1A–D); this associates with altered bone mechanical properties and perturbed osteocyte functions [13, 14, 21, 25, 32]. Cementocytes and their perilacunar regions in *Hyp* mice may be similarly affected, though functional changes are less clear [13, 14]. We aimed to determine whether *Spp1*/OPN ablation could correct the abnormal lacunocanalicular system (LCS) organization in *Hyp* mice.

Ploton silver staining of coronal sections of M1 and associated alveolar bone was performed to visualize and measure the osteocyte and cementocyte LCS [14]. Overall, silver staining showed large areas of osteoid in *Hyp* and *Hyp;Spp1*$^{-/-}$ alveolar bone, visualized as unstained and lightly stained regions compared to controls (Fig. 3A). Abnormal osteocytes/lacunae in both *Hyp* and *Hyp;Spp1*$^{-/-}$ mice showed dense silver staining surrounding the lacunae indicating POLs. In some instances, abnormal and closely located osteocyte lacunae in *Hyp* groups appeared to merge with one other and fuse to form an atypical larger space. Increased OPN localization paralleled these osteocyte perilacunar defects in *Hyp* mice (Fig. 3B). WT and *Spp1*$^{-/-}$ mouse alveolar bone showed normal osteocyte density and lacunocanalicular morphology (Fig. 3A, C). *Hyp* and *Hyp;Spp1*$^{-/-}$ mice showed reduced osteocyte density compared to WT and/or *Spp1*$^{-/-}$ mice in alveolar bone. Compared to controls, *Hyp* and *Hyp;Spp1*$^{-/-}$ mice showed significant alterations or trends including increased lacunar area, height and width, and decreased canaliculi lengths and reduced

numbers of canaliculi per osteocyte. Notably, despite the absence of OPN, the *Hyp;Spp1*$^{-/-}$ mouse alveolar bone osteocyte LCS remained defective.

3.3. High-phosphate diet improves dentoalveolar defects in Hyp mice independent of Spp1 (OPN) ablation

Conventional therapy for XLH involves treatment with supplements of oral phosphate (P_i) and calcitriol (the active form of vitamin D). The high-P_i (HP) diet increased serum P_i and reduced osteoid in *Hyp* long bones [33, 34], and increased serum P_i in *Hyp* and *Hyp;Spp1*$^{-/-}$ mice and normalized osteomalacia in tibias of double-deficient mice [25]. We aimed to determine whether HP diet in combination with *Spp1*/OPN ablation could correct dentoalveolar mineralization defects in *Hyp* mice, compared to the control diet (CTR) described above.

Micro-CT analysis showed no substantial differences in dentoalveolar tissue volumes or densities between WT and *Spp1*$^{-/-}$ mice on the HP diet (Fig. 4). No significant differences in enamel volume and density were observed between *Hyp* or *Hyp;Spp1*$^{-/-}$ mice vs. WT mice on the HP diet. However, even on the HP diet, *Hyp* and *Hyp;Spp1*$^{-/-}$ mice showed persistent reduced dentin volumes (16%) and densities (4–5%) compared to WT and/or *Spp1*$^{-/-}$ mice, and dental pulp volumes remained about double those in WT and *Spp1*$^{-/-}$ mice. Notably, *Hyp;Spp1*$^{-/-}$ mice showed an 8% increase in alveolar bone BV/TV compared with *Hyp* mice, in addition to a 12% and 7% increase in BV/TV in WT and *Spp1*$^{-/-}$ mice, respectively. BMD remained reduced (6–7%) in *Hyp* and *Hyp;Spp1*$^{-/-}$ mice vs. WT and/or *Spp1*$^{-/-}$ mice. No differences were detected in PDL volume among experimental groups on the HP diet. Because of improved mineralization in the HP-fed mice associated with partially corrected hypophosphatemia, cellular cementum could be analyzed by micro-CT. While cementum volume was not different among experimental groups, persistently decreased cellular cementum density was found in *Hyp* and *Hyp;Spp1*$^{-/-}$ mice vs. WT and/or *Spp1*$^{-/-}$ mice.

Histology showed partially normalized appearance of M1 tooth structures and associated alveolar bone with improved PDL attachment in *Hyp* and *Hyp;Spp1*$^{-/-}$ mice compared to control mice on the HP diet (Fig. 5). *Hyp* and *Hyp;Spp1*$^{-/-}$ mice exhibited persistently thinner dentin and a trend of widened predentin, but differences were reduced by the HP diet (compare to Fig. 2). ImageJ color map quantification based on H&E stain intensities showed comparable appearances of cellular cementum among experimental groups suggesting improved mineralization (Fig. 5 and Supplemental Fig. S1B).

Effects of *Spp1* genotype on *Hyp* mouse dentoalveolar defects were analyzed in Figures 1 and 2. We also evaluated effects of diet and genotype-diet interaction. HP diet significantly ameliorated mineralization defects in *Hyp* and *Hyp;Spp1*$^{-/-}$ mice, partially normalizing alveolar bone volume and density, pulp volume, PDL volume, predentin thickness, and cementoid/cementum ratio (Figure 6). These measurements also showed statistically significant interaction effects of genotype and diet. Because dentin and cellular cementum volumes and densities were analyzed differently on CTR vs. HP diet, these could not be directly compared for diet and interaction effects.

3.4. Improvement of the bone lacunocanalicular system in Hyp mice fed a high-phosphate diet

We aimed to determine whether the HP diet in combination with *Spp1*/OPN ablation could correct the abnormal lacunocanalicular system (LCS) organization in *Hyp* mice. In mice fed the HP diet, no significant differences were detected in lacunar area, height, or width, nor in canalicular length and/or canaliculi number per osteocyte (Fig. 7A, C). Notably, the HP diet was associated with robust localization of OPN in alveolar bone of both WT and *Hyp* mice (Fig. 7B). In general, similar LCS patterns were observed in osteocytes of mandibular bone (Supplemental Fig. S2). However, the HP diet failed to normalize canalicular number per individual mandibular osteocyte in *Hyp* and *Hyp;Spp1*$^{-/-}$ mice vs. control mice. No differences were found between genotypes in cementocyte density, lacunar area, height, or width; therefore, any effects of the HP vs. CTR diet were inconclusive (Supplemental Fig. S3).

We also evaluated effects of diet and genotype-diet interaction on alveolar bone lacunocanalicular properties. While ANOVA indicated a statistically significant effect associated with diet, there were few significantly different pairwise comparisons between any measurements in CTR vs. HP diet (Fig. 8). Interactions were only significant for lacunar area and height.

4. Discussion

We hypothesized that genetic ablation of osteopontin (*Spp1*/OPN) in the *Hyp* mouse model of X-linked hypophosphatemia (XLH) would reduce dentoalveolar mineralization defects, and we analyzed the effects of *Spp1* ablation in the context of both a control (CTR) and a high-P_i (HP) diet. Immunostaining confirmed increased OPN localization in *Hyp* vs. wild-type (WT) alveolar bone, particularly noticeable in the hypomineralized perilacunar osteocytic lesions (POLs). However, genetic ablation of *Spp1* in *Hyp* mice (*Hyp;Spp1*$^{-/-}$) fed the CTR diet did not reduce defects in enamel, dentin and alveolar bone, and it did not correct the perturbed features of the osteocyte lacunocanalicular system. On the HP diet, both *Hyp* and *Hyp;Spp1*$^{-/-}$ mice showed improved mineralization of enamel, dentin and alveolar bone, and they had normalized osteocyte lacunocanalicular measurements, despite inducing increased OPN in WT and *Hyp* mice. Statistical interaction between genotype and diet likely reflects that *Spp1* expression is highly responsive to P_i and genetic ablation of Spp1/OPN would remove that effect. Collectively, these data suggest that OPN is not a major contributor to dentoalveolar mineralization defects in *Hyp* mice, and that increasing P_i in *Hyp* mice partially corrects many dentoalveolar parameters. Thus, there appear to be other, as yet undetermined, compensatory mineralization mechanisms that arise from knockout of *Spp1*/OPN in the *Hyp* background.

4.1. Systemic and local contributions to mineralization defects in XLH/Hyp

Conventional therapy for XLH, consisting of oral $1,25(OH)_2D_3$ and P_i treatment, shows limited improvement in skeletal and dental defects, driving FGF23 even higher and leading to hypercalcemia and nephrocalcinosis [6, 35, 36]. A recent FGF23-neutralizing antibody (FGF23Ab) treatment targeting excess FGF23 is poised to become standard-of-

care. FGF23Ab (burosumab) improved biochemical and skeletal manifestations in *Hyp* mice [37] and in clinical trials [8]. Neither preclinical nor clinical trials of FGF23Ab directly evaluated dentoalveolar tissues. Evaluations of the effects of burosumab on dentoalveolar manifestations have been mixed to date with reports of either increased or decreased incidence of dental abscesses [8, 10, 11]. For dentoalveolar mineralization in *Hyp* mice, FGF23Ab treatment made very limited improvements (similar to 1,25D treatment), leaving persistent alveolar bone and dentin defects and dental abscesses [14]. The inability of FGF23Ab and $1,25(OH)_2D_3$ therapies to resolve XLH/*Hyp* mineralization defects reflects gaps in our knowledge about the functions of PHEX and pathologic mechanisms of XLH, which prevents effective, complete treatments.

The secreted, extracellular matrix phosphoprotein osteopontin (OPN, gene *SPP1*) regulates and inhibits mineralization *in vitro* and *in vivo* [15, 16, 38]. Gene editing studies in mice support that OPN particularly affects dentin and alveolar bone formation [17]. PHEX cleaves OPN to inactivate its mineralization-inhibiting properties [18–20, 39–41]. Increased OPN in bones and teeth in XLH patients and in *Hyp* mice likely inhibits mineralization [21–24, 42]. Thus, disruptions at both systemic (high FGF23, low $1,25(OH)_2D_3$ and P_i) and local (increased OPN) levels contribute to mineralization disorders in XLH, and to date, increased OPN levels have not been addressed by treatment approaches. Genetic deletion of OPN in *Hyp* mice partially improved mineralization in tibias and vertebrae independent of systemic mineral metabolism, though calvariae were resistant to improvement [25], so some effects appear to be regional. Administration of the HP diet further normalized osteomalacia in *Hyp;Spp1*$^{-/-}$, pointing to roles for both OPN and P_i in XLH/*Hyp*-associated mineralization defects. In terms of the characteristic hypomineralized periosteocytic lesions (POLs), reducing OPN or increasing P_i, either independently or simultaneously, did not resolve POLs in long bones. Dysregulation of pyrophosphate (PP_i) pathways in osteocytes, particularly in response to a HP diet, likely contributes to persistent POLs.

4.2. Contributions of OPN and hypophosphatemia to XLH/Hyp-associated dentoalveolar mineralization defects

In the first part of this study, ablation of *Spp1*/OPN made no measurable improvements to enamel, dentin, or alveolar bone mineralization defects in *Hyp;Spp1*$^{-/-}$ vs. *Hyp* mice. POLs were similarly unimproved in postcranial bones by OPN ablation in our previous study [25]. The sole exception was cellular cementum, where the proportion of hypomineralized cementoid in *Hyp* mice was reduced by knocking out OPN. It is not clear as to why cellular cementum mineralization defects were ameliorated by deletion of *Spp1*/OPN whereas dentin and bone were not responsive. One possibility may be that because *Phex* expression is much higher in odontoblasts, osteoblasts, and osteocytes than in cementoblasts and cementocytes [13, 43], there may local, direct effects of PHEX loss-of-function in these tissues that cannot be overridden by reduction in OPN.

In our previous study, OPN ablation in *Hyp* mice improved mineralization of tibias and vertebrae, particularly trabecular bone parameters, but failed to improve calvarial mineralization [25]. Lack of improvement in the majority of *Hyp* mouse dentoalveolar tissues from ablation of OPN suggests several possible explanations. It is possible (and even

likely) that OPN is not the only nascent, full-length substrate for PHEX in mineralized tissues. Other members of the Small Integrin Binding Ligand N-linked Glycoprotein (SIBLING) family, like OPN, harbor acidic serine- and aspartate-rich motifs (ASARM peptides) that function as mineralization inhibitors. ASARM peptides from OPN, matrix extracellular phosphoglycoprotein (MEPE), and dentin matrix protein 1 (DMP1) are substrates for PHEX [18, 19, 23, 24, 39]. Individually, or collectively, it is possible that accumulation of such inhibitory peptides may contribute to mineralization defects in XLH. Unlike the postcranial skeleton, the dentoalveolar hard tissues are produced by neural crest-derived ectomesenchymal cells (except for the epithelium-derived enamel) and may rely on other mineralization regulators in addition to OPN. Other compensatory regulators may be triggered by *Spp1* ablation, particularly progressive ankylosis protein (*Ank*/ANK) and ectonucleotide pyrophosphatase phosphodiesterase (*Enpp1*/ENPP1), which can regulate mineralization by increasing local PP_i levels, complicating analysis and interpretation [44]. While OPN is implicated as a regulator of dentoalveolar development [17], deletion of OPN failed to substantially impact dentoalveolar phenotypes in other models of mineral dysregulation (*e.g.* $Alpl^{-/-}$ and $Ank^{-/-}$ mice) [17], suggesting a more complex and potentially limited role in this region. Similar to calvarial bone, alveolar bone undergoes intramembranous ossification, and may be subject to different mineralization regulators than those governing endochondral ossification. In particular, persistent hypophosphatemia in $Hyp;Spp1^{-/-}$ mice prompted studies comparing the effects of HP to CTR diet.

The HP diet led to a more dramatic improvement in dentoalveolar mineralization in *Hyp* mice, regardless of ablation of *Spp1*/OPN. Bulk mineralization of enamel, dentin, and alveolar bone were nearly normalized to controls, with some persistent defects including increased dental pulp volume and reduced cellular cementum density by micro-CT. Unlike analyses of the postcranial skeleton, POLs and other lacuna-canalicular abnormalities in alveolar and mandibular bone of *Hyp* and $Hyp;Spp1^{-/-}$ mice were largely resolved by the HP diet. These combined results support hypophosphatemia as a major contributor to a range of dentoalveolar defects in XLH, with negligible contributions from OPN in this cranial context. These findings are in line with many previous studies indicating that dentoalveolar tissues are highly sensitive to perturbations of P_i/PP_i metabolism, exemplified by *in vitro* studies of P_i signaling [45] and inherited disorders such as hypophosphatasia (HPP) [46]. Notably, HP appeared to more effective for treatment of dentoalveolar defects than a previous study employing $1,25(OH)_2D_3$ or FGF23Ab [14].

Statistical interactions between genotype and diet indicated by two-way ANOVA implicate interplay between these two variables. This likely, in part, reflects the regulation of Spp1/OPN expression by P_i [47–49]. The complex crosstalk between systemic regulators of mineral metabolism (*e.g.* FGF23, $1,25(OH)_2D_3$, and parathyroid hormone) and local regulators of mineral metabolism (*e.g.* OPN, ANK, ENPP1 and TNAP) make it challenging to conduct and interpret studies of the functions of individual factors. Additional studies should investigate PP_i metabolism in the dentoalveolar manifestations of XLH, and they should include functional tests such as periodontal mechanical properties or prevalence of abscesses when evaluating potential therapies.

Supplementary Material

Refer to Web version on PubMed Central for supplementary material.

Funding

This study was supported by a grant from the Canadian Institutes of Health Research (CIHR) to MDM (Grant MOP-142330) and by a grant from the National Institute of Dental and Craniofacial Research (NIDCR) to BLF (Grant R01DE032334). This work was also supported funding from the provincial FRQS Network for Oral and Bone Health Research (to MDM and MM), and by a doctoral training award from the Fonds de la Recherche en Santé du Québec (to BH, 28308). MDM is the Canada Research Chair in Biomineralization, and this research was undertaken, in part, thanks to funding from the Canada Research Chairs program.

Data availability

Data will be made available on request.

References

[1]. Carpenter TO, Imel EA, Holm IA, Jan de Beur SM, Insogna KL, A clinician's guide to X-linked hypophosphatemia, J Bone Miner Res 26(7) (2011) 1381–8. [PubMed: 21538511]

[2]. Francis F, Hennig S, Korn B, Reinhardt R, de Jong P, Poustka A, Lehrach H, Rowe PSN, Goulding JN, Summerfield T, Mountford R, Read AP, Popowska E, Pronicka E, Davies KE, O'Riordan JLH, Econs MJ, Nesbitt T, Drezner MK, Oudet C, Pannetier S, Hanauer A, Strom TM, Meindl A, Lorenz B, Cagnoli B, Mohnike KL, Murken J, Meitinger T, A gene (PEX) with homologies to endopeptidases is mutated in patients with X-linked hypophosphatemic rickets. The HYP Consortium, Nat Genet 11(2) (1995) 130–6. [PubMed: 7550339]

[3]. Coyac BR, Falgayrac G, Penel G, Schmitt A, Schinke T, Linglart A, McKee MD, Chaussain C, Bardet C, Impaired mineral quality in dentin in X-linked hypophosphatemia, Connect Tissue Res 59(sup1) (2018) 91–96. [PubMed: 29745817]

[4]. Clayton D, Chavez MB, Tan MH, Kolli TN, Giovani PA, Hammersmith KJ, Bowden SA, Foster BL, Mineralization Defects in the Primary Dentition Associated With X-Linked Hypophosphatemic Rickets, JBMR Plus 5(4) (2021) e10463. [PubMed: 33869987]

[5]. Foster BL, Nociti FH Jr., Somerman MJ, The rachitic tooth, Endocr Rev 35(1) (2014) 1–34. [PubMed: 23939820]

[6]. Biosse Duplan M, Coyac BR, Bardet C, Zadikian C, Rothenbuhler A, Kamenicky P, Briot K, Linglart A, Chaussain C, Phosphate and Vitamin D Prevent Periodontitis in X-Linked Hypophosphatemia, J Dent Res 96(4) (2017) 388–395. [PubMed: 27821544]

[7]. Carpenter TO, Whyte MP, Imel EA, Boot AM, Hogler W, Linglart A, Padidela R, Van't Hoff W, Mao M, Chen CY, Skrinar A, Kakkis E, San Martin J, Portale AA, Burosumab Therapy in Children with X-Linked Hypophosphatemia, N Engl J Med 378(21) (2018) 1987–1998. [PubMed: 29791829]

[8]. Imel EA, Glorieux FH, Whyte MP, Munns CF, Ward LM, Nilsson O, Simmons JH, Padidela R, Namba N, Cheong HI, Pitukcheewanont P, Sochett E, Hogler W, Muroya K, Tanaka H, Gottesman GS, Biggin A, Perwad F, Mao M, Chen CY, Skrinar A, San Martin J, Portale AA, Burosumab versus conventional therapy in children with X-linked hypophosphataemia: a randomised, active-controlled, open-label, phase 3 trial, Lancet 393(10189) (2019) 2416–2427. [PubMed: 31104833]

[9]. Imel EA, Burosumab for Pediatric X-Linked Hypophosphatemia, Curr Osteoporos Rep 19(3) (2021) 271–277. [PubMed: 33970403]

[10]. Gadion M, Herve A, Herrou J, Rothenbuhler A, Smail-Faugeron V, Courson F, Linglart A, Chaussain C, Biosse Duplan M, Burosumab and Dental Abscesses in Children With X-Linked Hypophosphatemia, JBMR Plus 6(11) (2022) e10672. [PubMed: 36398111]

[11]. Brener R, Zeitlin L, Lebenthal Y, Brener A, Dental health of pediatric patients with X-linked hypophosphatemia (XLH) after three years of burosumab therapy, Front Endocrinol (Lausanne) 13 (2022) 947814. [PubMed: 36051396]

[12]. Ward LM, Glorieux FH, Whyte MP, Munns CF, Portale AA, Hogler W, Simmons JH, Gottesman GS, Padidela R, Namba N, Cheong HI, Nilsson O, Mao M, Chen A, Skrinar A, Roberts MS, Imel EA, Effect of Burosumab Compared With Conventional Therapy on Younger vs Older Children With X-linked Hypophosphatemia, J Clin Endocrinol Metab 107(8) (2022) e3241–e3253. [PubMed: 35533340]

[13]. Zhang H, Chavez MB, Kolli TN, Tan MH, Fong H, Chu EY, Li Y, Ren X, Watanabe K, Kim DG, Foster BL, Dentoalveolar Defects in the Hyp Mouse Model of X-linked Hypophosphatemia, J Dent Res 99(4) (2020) 419–428. [PubMed: 31977267]

[14]. Lira Dos Santos EJ, Chavez MB, Tan MH, Mohamed FF, Kolli TN, Foster BL, Liu ES, Effects of Active Vitamin D or FGF23 Antibody on Hyp Mice Dentoalveolar Tissues, J Dent Res (2021) 220345211011041.

[15]. Boskey AL, Spevak L, Paschalis E, Doty SB, McKee MD, Osteopontin deficiency increases mineral content and mineral crystallinity in mouse bone, Calcif Tissue Int 71(2) (2002) 145–54. [PubMed: 12073157]

[16]. Sodek J, Ganss B, McKee MD, Osteopontin, Crit Rev Oral Biol Med 11(3) (2000) 279–303. [PubMed: 11021631]

[17]. Foster BL, Ao M, Salmon CR, Chavez MB, Kolli TN, Tran AB, Chu EY, Kantovitz KR, Yadav M, Narisawa S, Millan JL, Nociti FH Jr., Somerman MJ, Osteopontin regulates dentin and alveolar bone development and mineralization, Bone 107 (2018) 196–207. [PubMed: 29313816]

[18]. Addison W, Masica D, Gray J, McKee M, Phosphorylation-dependent inhibition of mineralization by osteopontin ASARM peptides is regulated by PHEX cleavage., J Bone Miner Res 25(4) (2010) 695–705. [PubMed: 19775205]

[19]. Addison W, Nakano Y, Loisel T, Crine P, McKee M, MEPE-ASARM peptides control extracellular matrix mineralization by binding to hydroxyapatite: an inhibition regulated by PHEX cleavage of ASARM., J Bone Miner Res 23(10) (2008) 1638–49. [PubMed: 18597632]

[20]. Barros NM, Hoac B, Neves RL, Addison WN, Assis DM, Murshed M, Carmona AK, McKee MD, Proteolytic processing of osteopontin by PHEX and accumulation of osteopontin fragments in Hyp mouse bone, the murine model of X-linked hypophosphatemia, J Bone Miner Res (2012).

[21]. Boukpessi T, Hoac B, Coyac BR, Leger T, Garcia C, Wicart P, Whyte MP, Glorieux FH, Linglart A, Chaussain C, McKee MD, Osteopontin and the dento-osseous pathobiology of X-linked hypophosphatemia, Bone 95 (2017) 151–161. [PubMed: 27884786]

[22]. Coyac BR, Falgayrac G, Baroukh B, Slimani L, Sadoine J, Penel G, Biosse-Duplan M, Schinke T, Linglart A, McKee MD, Chaussain C, Bardet C, Tissue-specific mineralization defects in the periodontium of the Hyp mouse model of X-linked hypophosphatemia, Bone 103 (2017) 334–346. [PubMed: 28764922]

[23]. Salmon B, Bardet C, Coyac BR, Baroukh B, Naji J, Rowe PS, Opsahl Vital S, Linglart A, McKee MD, Chaussain C, Abnormal osteopontin and matrix extracellular phosphoglycoprotein localization, and odontoblast differentiation, in X-linked hypophosphatemic teeth, Connect Tissue Res 55 Suppl 1 (2014) 79–82. [PubMed: 25158186]

[24]. Barros NM, Hoac B, Neves RL, Addison WN, Assis DM, Murshed M, Carmona AK, McKee MD, Proteolytic processing of osteopontin by PHEX and accumulation of osteopontin fragments in Hyp mouse bone, the murine model of X-linked hypophosphatemia, J Bone Miner Res 28(3) (2013) 688–99. [PubMed: 22991293]

[25]. Hoac B, Ostergaard M, Wittig NK, Boukpessi T, Buss DJ, Chaussain C, Birkedal H, Murshed M, McKee MD, Genetic Ablation of Osteopontin in Osteomalacic Hyp Mice Partially Rescues the Deficient Mineralization Without Correcting Hypophosphatemia, J Bone Miner Res 35(10) (2020) 2032–2048. [PubMed: 32501585]

[26]. Lira Dos Santos EJ, Chavez MB, Tan MH, Mohamed FF, Kolli TN, Foster BL, Liu ES, Effects of Active Vitamin D or FGF23 Antibody on Hyp Mice Dentoalveolar Tissues, J Dent Res 100(13) (2021) 1482–1491. [PubMed: 33906518]

[27]. Chavez MB, Chu EY, Kram V, de Castro LF, Somerman MJ, Foster BL, Guidelines for Micro-Computed Tomography Analysis of Rodent Dentoalveolar Tissues, JBMR Plus 5(3) (2021) e10474. [PubMed: 33778330]

[28]. Foster BL, Methods for studying tooth root cementum by light microscopy, Int J Oral Sci 4(3) (2012) 119–28. [PubMed: 22996273]

[29]. Foster BL, Soenjaya Y, Nociti FH Jr., Holm E, Zerfas PM, Wimer HF, Holdsworth DW, Aubin JE, Hunter GK, Goldberg HA, Somerman MJ, Deficiency in acellular cementum and periodontal attachment in bsp null mice, J Dent Res 92(2) (2013) 166–72. [PubMed: 23183644]

[30]. Foster BL, Nagatomo KJ, Nociti FH Jr., Fong H, Dunn D, Tran AB, Wang W, Narisawa S, Millan JL, Somerman MJ, Central role of pyrophosphate in acellular cementum formation, PLoS One 7(6) (2012) e38393. [PubMed: 22675556]

[31]. Foster BL, Nagatomo KJ, Bamashmous SO, Tompkins KA, Fong H, Dunn D, Chu EY, Guenther C, Kingsley DM, Rutherford RB, Somerman MJ, The progressive ankylosis protein regulates cementum apposition and extracellular matrix composition, Cells Tissues Organs 194(5) (2011) 382–405. [PubMed: 21389671]

[32]. Tokarz D, Martins JS, Petit ET, Lin CP, Demay MB, Liu ES, Hormonal Regulation of Osteocyte Perilacunar and Canalicular Remodeling in the Hyp Mouse Model of X-Linked Hypophosphatemia, J Bone Miner Res 33(3) (2018) 499–509. [PubMed: 29083055]

[33]. Marie PJ, Travers R, Glorieux FH, Healing of rickets with phosphate supplementation in the hypophosphatemic male mouse, J Clin Invest 67(3) (1981) 911–4. [PubMed: 6259210]

[34]. Murshed M, Harmey D, Millan JL, McKee MD, Karsenty G, Unique coexpression in osteoblasts of broadly expressed genes accounts for the spatial restriction of ECM mineralization to bone, Genes Dev 19(9) (2005) 1093–104. [PubMed: 15833911]

[35]. Chaussain-Miller C, Sinding C, Septier D, Wolikow M, Goldberg M, Garabedian M, Dentin structure in familial hypophosphatemic rickets: benefits of vitamin D and phosphate treatment., Oral Dis 13(5) (2007) 482–9. [PubMed: 17714351]

[36]. Connor J, Olear EA, Insogna KL, Katz L, Baker S, Kaur R, Simpson CA, Sterpka J, Dubrow R, Zhang JH, Carpenter TO, Conventional Therapy in Adults With X-Linked Hypophosphatemia: Effects on Enthesopathy and Dental Disease, J Clin Endocrinol Metab 100(10) (2015) 3625–32. [PubMed: 26176801]

[37]. Aono Y, Yamazaki Y, Yasutake J, Kawata T, Hasegawa H, Urakawa I, Fujita T, Wada M, Yamashita T, Fukumoto S, Shimada T, Therapeutic effects of anti-FGF23 antibodies in hypophosphatemic rickets/osteomalacia, J Bone Miner Res 24(11) (2009) 1879–88. [PubMed: 19419316]

[38]. McKee MD, Buss DJ, Reznikov N, Mineral tessellation in bone and the stenciling principle for extracellular matrix mineralization, J Struct Biol 214(1) (2022) 107823. [PubMed: 34915130]

[39]. Martin A, David V, Laurence J, Schwarz P, Lafer E, Hedge A, Rowe P, Degradation of MEPE, DMP1, and release of SIBLING ASARM-peptides (minhibins): ASARM-peptide(s) are directly responsible for defective mineralization in HYP., Endocrinology 149(4) (2008) 1757–72. [PubMed: 18162525]

[40]. Rowe PS, Kumagai Y, Gutierrez G, Garrett IR, Blacher R, Rosen D, Cundy J, Navvab S, Chen D, Drezner MK, Quarles LD, Mundy GR, MEPE has the properties of an osteoblastic phosphatonin and minhibin, Bone 34(2) (2004) 303–19. [PubMed: 14962809]

[41]. Boukpessi T, Gaucher C, Léger T, Salmon B, Le Faouder J, Willig C, Rowe PS, Garabédian M, Meilhac O, Chaussain C, Abnormal presence of the matrix extracellular phosphoglycoprotein-derived acidic serine- and aspartate-rich motif peptide in human hypophosphatemic dentin., Am J Pathol 177(2) (2010) 803–12. [PubMed: 20581062]

[42]. Zhang B, Sun Y, Chen L, Guan C, Guo L, Qin C, Expression and distribution of SIBLING proteins in the predentin/dentin and mandible of hyp mice, Oral Dis 16(5) (2010) 453–64. [PubMed: 20233318]

[43]. Ruchon AF, Tenenhouse HS, Marcinkiewicz M, Siegfried G, Aubin JE, DesGroseillers L, Crine P, Boileau G, Developmental expression and tissue distribution of Phex protein: effect of the Hyp mutation and relationship to bone markers, J Bone Miner Res 15(8) (2000) 1440–50. [PubMed: 10934642]

[44]. Harmey D, Hessle L, Narisawa S, Johnson KA, Terkeltaub R, Millan JL, Concerted regulation of inorganic pyrophosphate and osteopontin by akp2, enpp1, and ank: an integrated model of the pathogenesis of mineralization disorders, Am J Pathol 164(4) (2004) 1199–209. [PubMed: 15039209]

[45]. Rutherford RB, Foster BL, Bammler T, Beyer RP, Sato S, Somerman MJ, Extracellular phosphate alters cementoblast gene expression, J Dent Res 85(6) (2006) 505–9. [PubMed: 16723645]

[46]. Bowden SA, Foster BL, Alkaline Phosphatase Replacement Therapy for Hypophosphatasia in Development and Practice, Adv Exp Med Biol 1148 (2019) 279–322. [PubMed: 31482504]

[47]. Fatherazi S, Matsa-Dunn D, Foster BL, Rutherford RB, Somerman MJ, Presland RB, Phosphate regulates osteopontin gene transcription, J Dent Res 88(1) (2009) 39–44. [PubMed: 19131315]

[48]. Foster BL, Nociti FH Jr., Swanson EC, Matsa-Dunn D, Berry JE, Cupp CJ, Zhang P, Somerman MJ, Regulation of cementoblast gene expression by inorganic phosphate in vitro, Calcif Tissue Int 78(2) (2006) 103–12. [PubMed: 16467974]

[49]. Beck GR Jr., Zerler B, Moran E, Phosphate is a specific signal for induction of osteopontin gene expression, Proc Natl Acad Sci U S A 97(15) (2000) 8352–7. [PubMed: 10890885]

Highlights

- Levels of osteopontin (Spp1/OPN), a mineralization inhibiting non-collagenous matrix protein, are increased in dentoalveolar tissues of the *Hyp* mutant mouse model of X-linked hypophosphatemia (XLH)
- Genetic ablation of *Spp1*/OPN in *Hyp* mice did not reduce mineralization defects in most dentoalveolar tissues
- High phosphate diet markedly improved many mineralization measurements in *Hyp* and *Hyp;Spp1* double deficient mouse dentoalveolar tissues, with some indication of interaction between genotype and diet

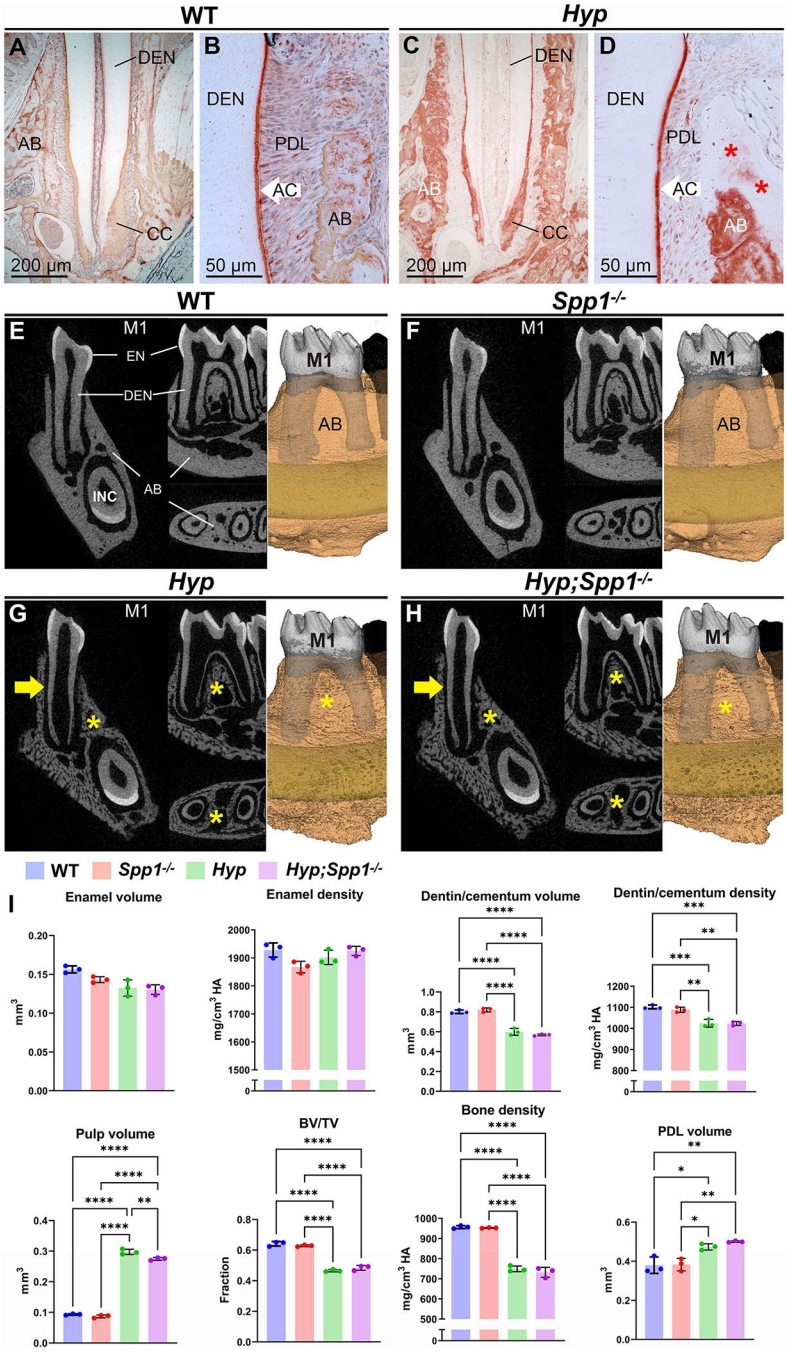

Fig. 1. Spp1 ablation in Hyp mice does not rescue most dentoalveolar defects.

(A-D) OPN immunohistochemistry shows increased and altered localization of OPN in *Hyp* vs. WT dentoalveolar tissues, particularly in alveolar bone (AB) and cellular cementum (CC). Red asterisks indicate unmineralized regions of alveolar bone (osteoid). AC/white arrows: Acellular cementum. (**E-H**) 2D and 3D renderings from micro-CT of mandibular first molar (M1) dentoalveolar structures showing comparable enamel (EN), thin dentin (DEN); yellow arrows in G, H), wide pulp chamber, wide periodontal ligament (PDL), and alveolar bone (AB) defects (yellow asterisks in G, H) in *Hyp* and *Hyp;Spp1*$^{-/-}$ mice

vs. WT and *Spp1*$^{-/-}$ controls. **(I)** Quantitative analysis of M1 dentoalveolar structures showing effects on DE/cementum, pulp, AB, and PDL. INC: Incisor. *P<0.05; **P<0.01; ***P<0.001; ****P<0.0001.

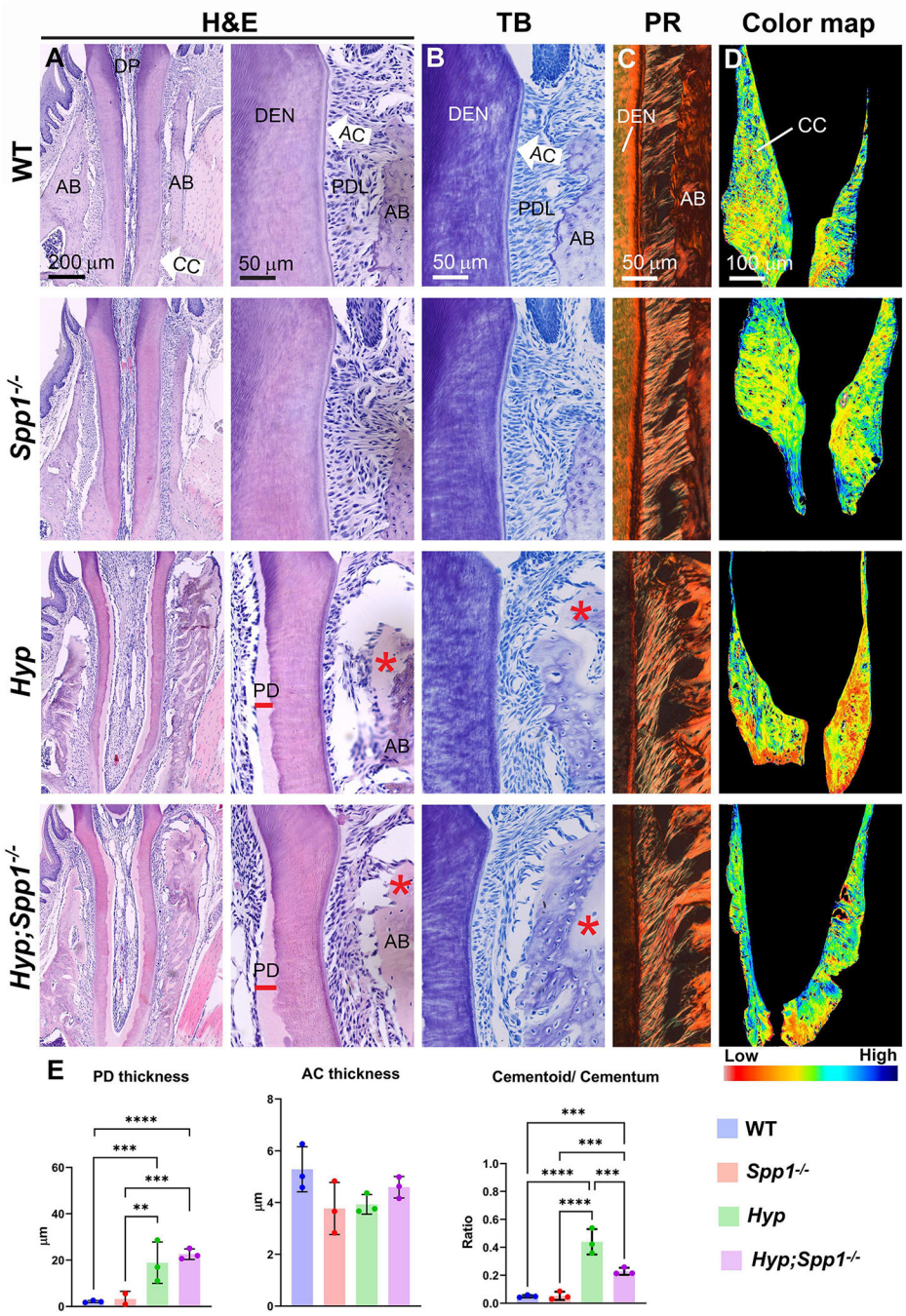

Fig. 2. Persistent alterations in dentin and periodontium in *Hyp* and *Hyp;Spp1*$^{-/-}$ mice.

(A) Hematoxylin and eosin (H&E) and **(B)** toluidine blue (TB) staining shows normal dentoalveolar tissues in *Spp1*$^{-/-}$ and WT mice, while both *Hyp* and *Hyp;Spp1*$^{-/-}$ mice exhibit thin dentin (DEN), widened predentin (PD), and osteoid accumulation (*) in alveolar bone (AB). Acellular cementum (AC) appears present in all genotypes. **(C)** Picrosirius red (PR) shows periodontal ligament (PDL) attachment and organization in all genotypes. **(D)** ImageJ color map quantification based on H&E stain intensities shows that *Hyp* mice exhibit larger regions of cementoid (red-orange) vs. mineralized (yellow-green-blue)

cellular cementum (CC), compared to other genotypes, with *Hyp;Spp1*$^{-/-}$ mice showing reduced cementoid. **(E)** Quantification of PD, AC, and cementoid/cementum measurements. ** $P<0.01$; *** $P<0.001$; **** $P<0.0001$.

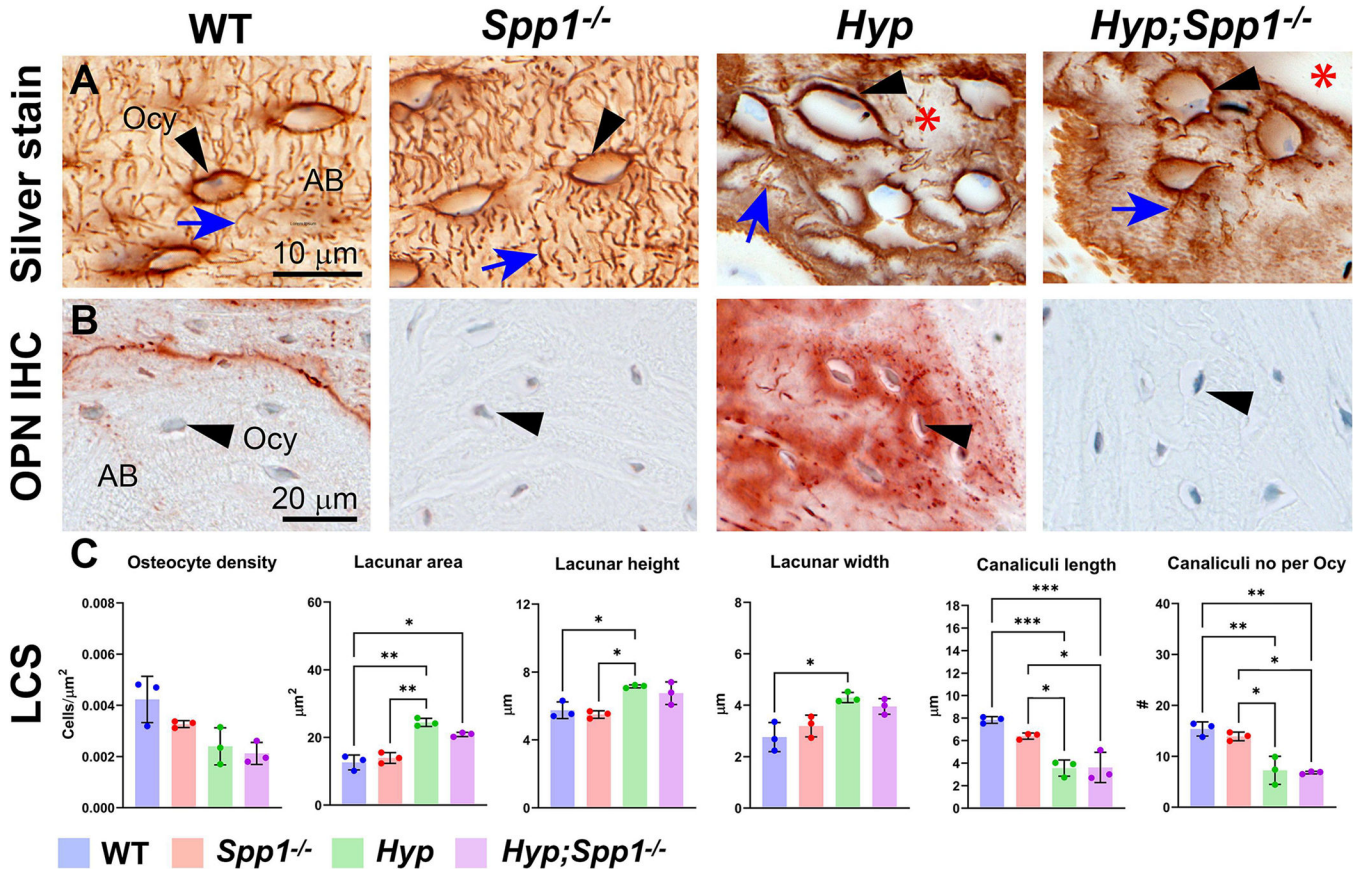

Fig. 3. *Spp1* ablation *in Hyp* mice does not ameliorate alveolar bone lacunocanalicular defects.

Silver staining is used to visualize and measure alveolar bone (AB) osteocyte (Ocy) lacunocanalicular systems (LCS). **(A)** Silver staining of AB/Ocy/LCS from mice where black arrowheads point to lacunae and blue arrows point to canaliculi. Accumulations of osteoid are indicated by red asterisks. **(B)** Immunohistochemical staining (red) shows increased perilacunar OPN localization in *Hyp* mouse AB and LCS. OPN is absent in mice where *Spp1* is ablated. **(C)** Measurements of the LCS show alterations in *Hyp* mice that are not corrected by *Spp1* ablation. **P*<0.05; ***P*<0.01; ****P*<0.001.

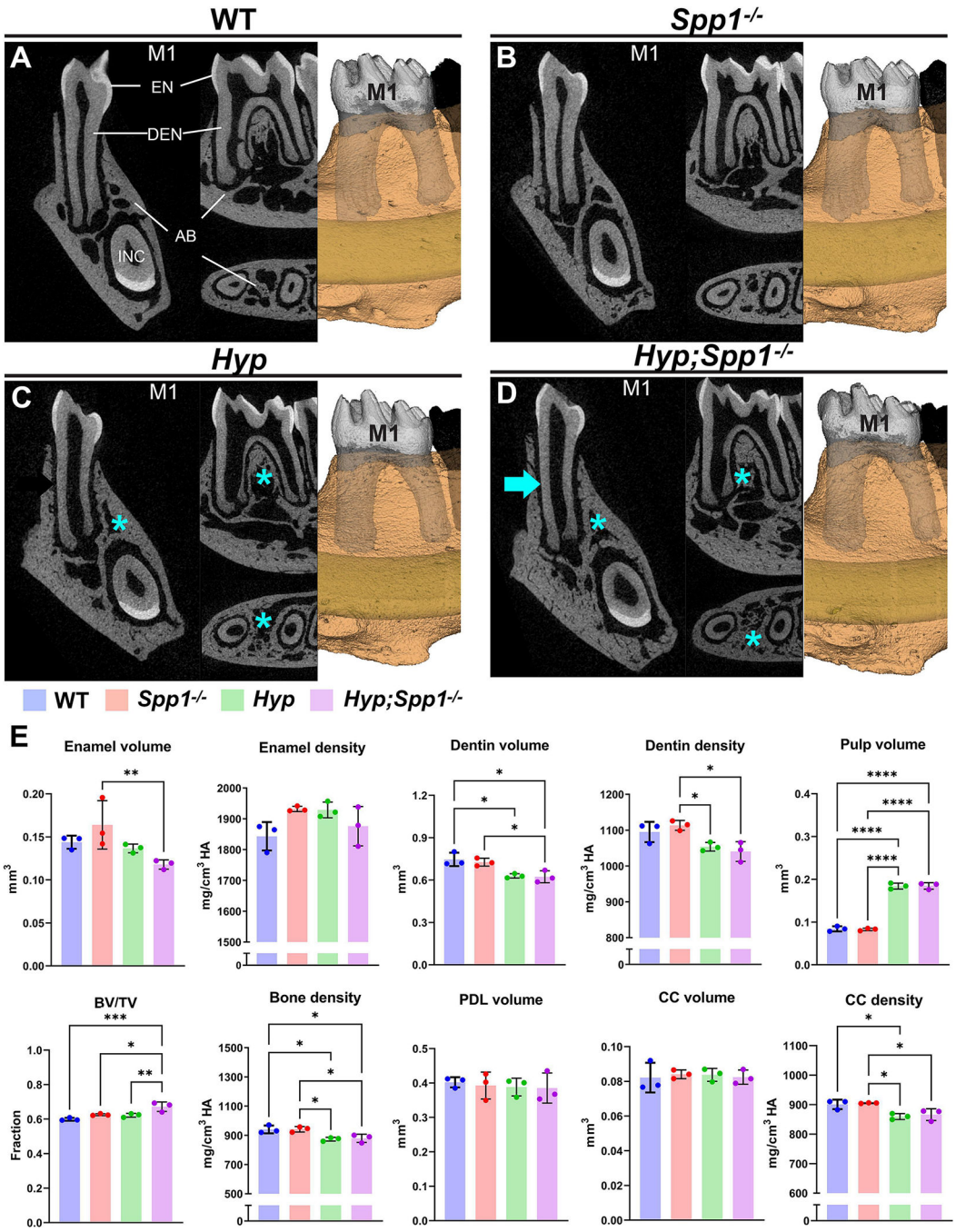

Fig. 4. High-phosphate diet improves dentoalveolar defects in *Hyp* mice independent of *Spp1* ablation.

(**A-D**) 2D and 3D renderings from micro-CT of mandibular first molar (M1) dentoalveolar structures showing the effects of high-phosphate diet on dentoalveolar defects in *Hyp* and *Hyp;Spp1*$^{-/-}$ mice, including increased dentin (DEN) thickness (cyan arrows in C, D) and improved alveolar bone (AB) mineralization (cyan asterisks in C, D) compared to *Hyp* mouse groups fed a standard diet (compare to Fig.1). (**E**) Quantitative analysis of M1 dentoalveolar structures showing residual effects on enamel (EN), DEN, pulp, and AB, and

cellular cementum (CC), and no differences between genotypes in periodontal ligament (PDL) volume. INC: Incisor. * $P<0.05$; ** $P<0.01$; *** $P<0.001$; **** $P<0.0001$.

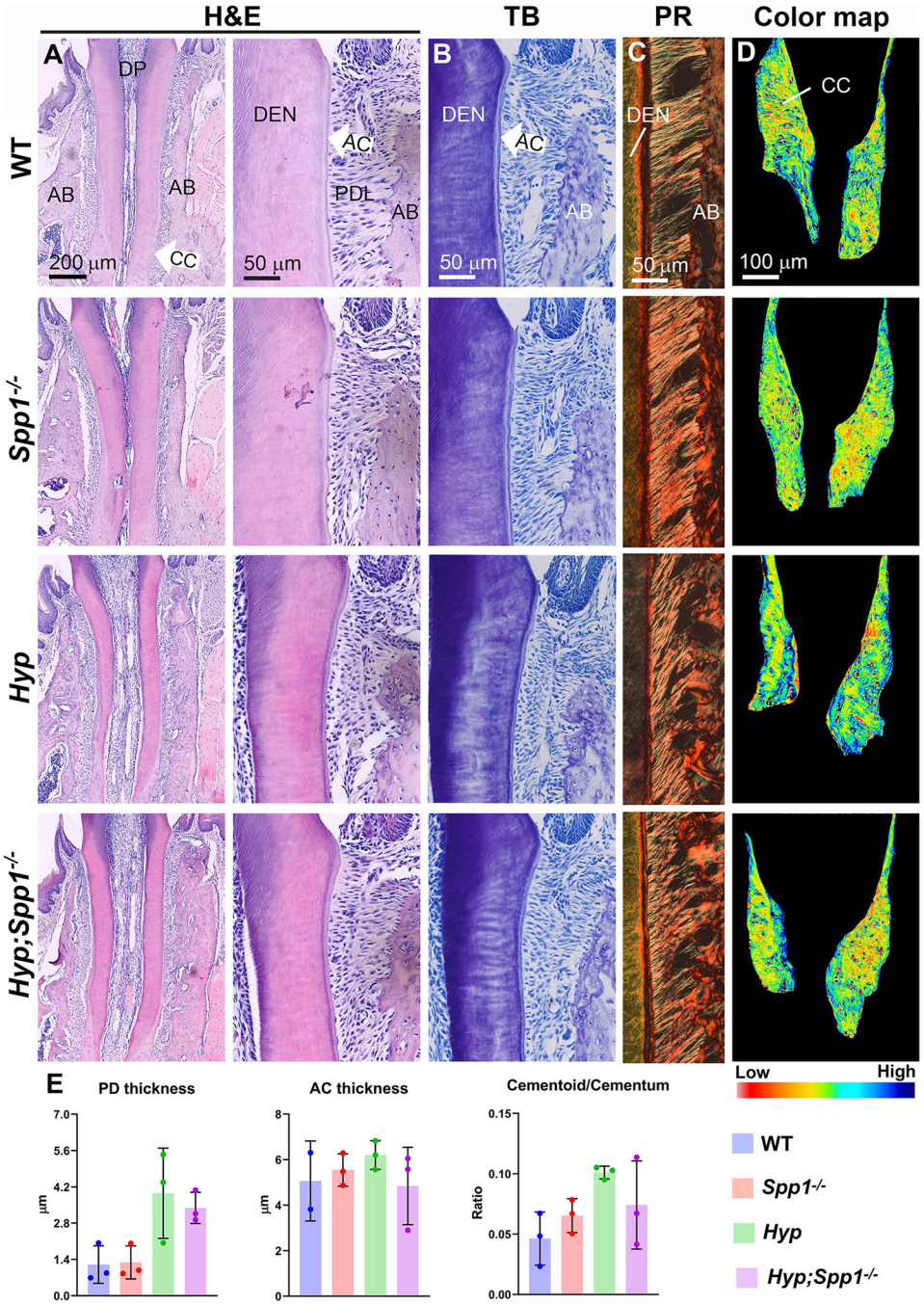

Fig. 5. Effect of high-phosphate diet on dentin, cementum, and bone defects in *Hyp* and *Hyp;Spp1*$^{-/-}$ mice.

(A) Hematoxylin and eosin (H&E) and **(B)** toluidine blue (TB) staining shows **the** partially normalized appearance of mandibular first molar (M1) dentin (DEN) and associated alveolar bone (AB) in *Hyp* and *Hyp;Spp1*$^{-/-}$ mice compared to control mice fed a high-phosphate (HP) diet. *Hyp* and *Hyp;Spp1*$^{-/-}$ mice exhibit thinner DEN and a trend towards wider predentin (PD) compared to control mice, but differences were reduced by the HP diet (compare to Fig. 2). **(C)** Picrosirius red staining (PR) shows periodontal ligament (PDL)

attachment and organization in all genotypes. **(D)** ImageJ color map quantification based on H&E stain intensities shows comparable appearances of cellular cementum (CC) among experimental groups (similar range of yellow-green-blue indicating little cementoid). (**E**) Quantification of PD, AC, and cementoid/cementum measurements. AC; Acellular cementum. *P<0.05.

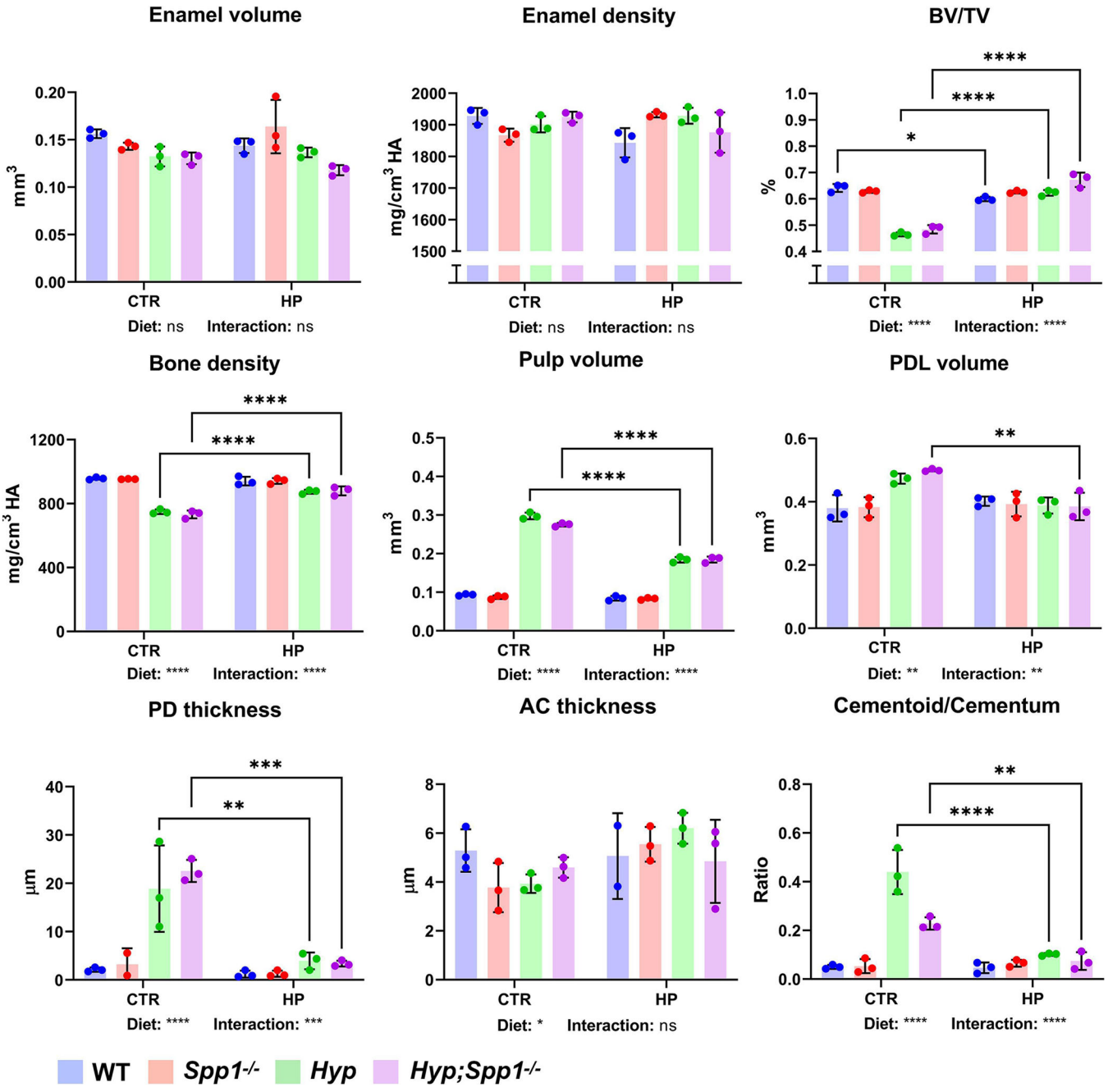

Fig. 6. Genotype-diet interactions in improved dentoalveolar properties of *Hyp* and *Hyp*;*Spp1*$^{-/-}$ mice.

Comparisons across diet (CTR vs. HP) are shown between mice of the same genotype. Comparisons between genotypes are shown in Figures 1 and 4. Two-way ANOVA with post-hoc Tukey test indicated statistically significant genotype-diet interactions in CTR vs. HP diets. *P*-values are shown for both diet and interactions beneath each graph. **P*<0.05; ***P*<0.01; ****P*<0.001; *****P*<0.0001.

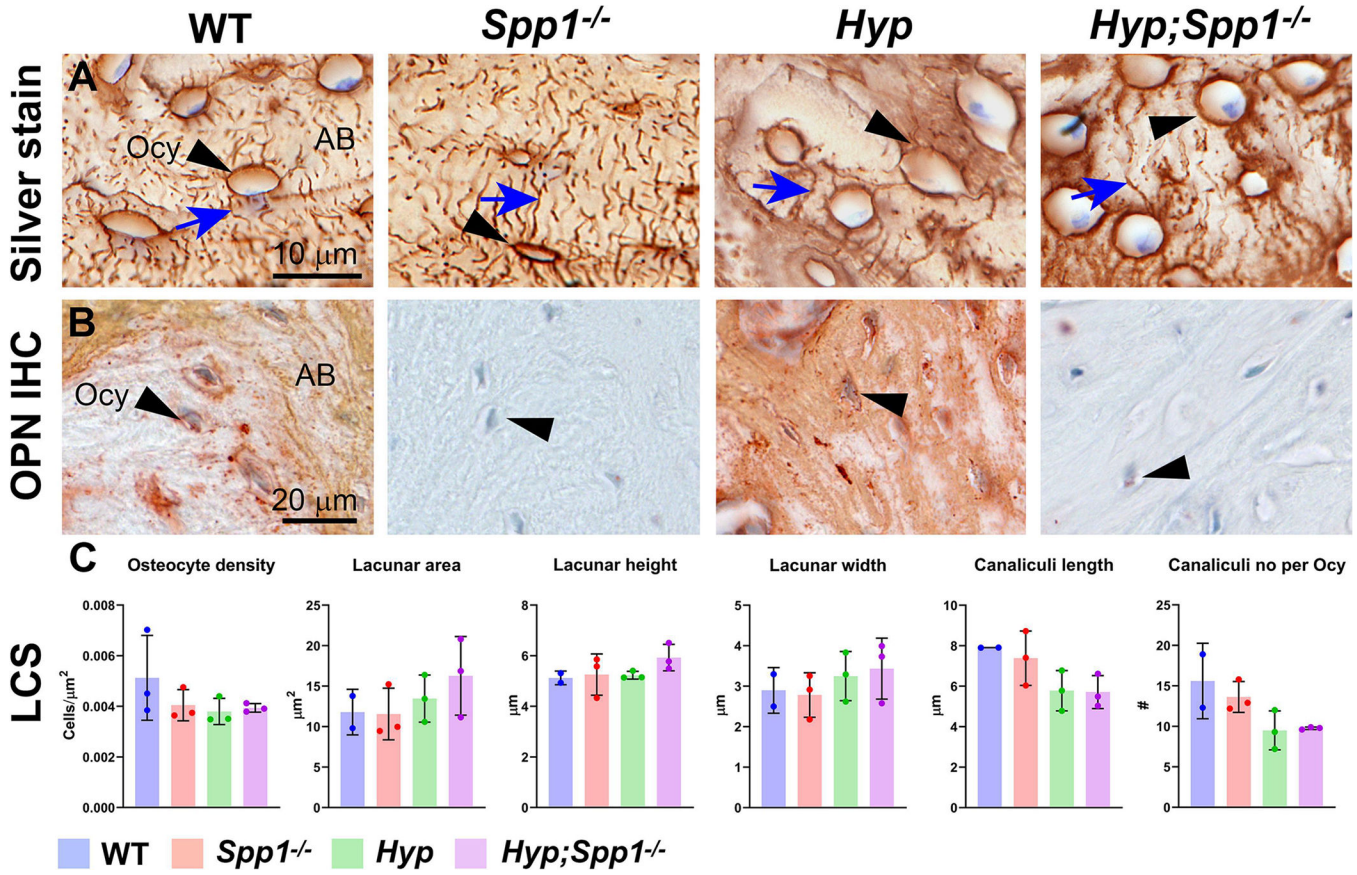

Fig. 7. Improvement of alveolar bone lacunocanalicular system in *Hyp* mice fed a high-phosphate diet.

Silver staining is used to visualize and measure alveolar bone (AB) osteocyte (Ocy) lacunocanalicular systems (LCS) for mice fed an HP diet. **(A)** Silver staining of Ab Ocy fed a HP diet where black arrowheads point to lacunae and blue arrows point to canaliculi. **(B)** Immunohistochemistry shows increased perilacunar OPN localization in *Hyp* mice and the HP diet generally increases OPN staining in AB, including around Ocy. OPN is absent in mice where *Spp1* is ablated. **(C)** Measurements of the LCS show no significant differences between genotypes fed a HP diet.

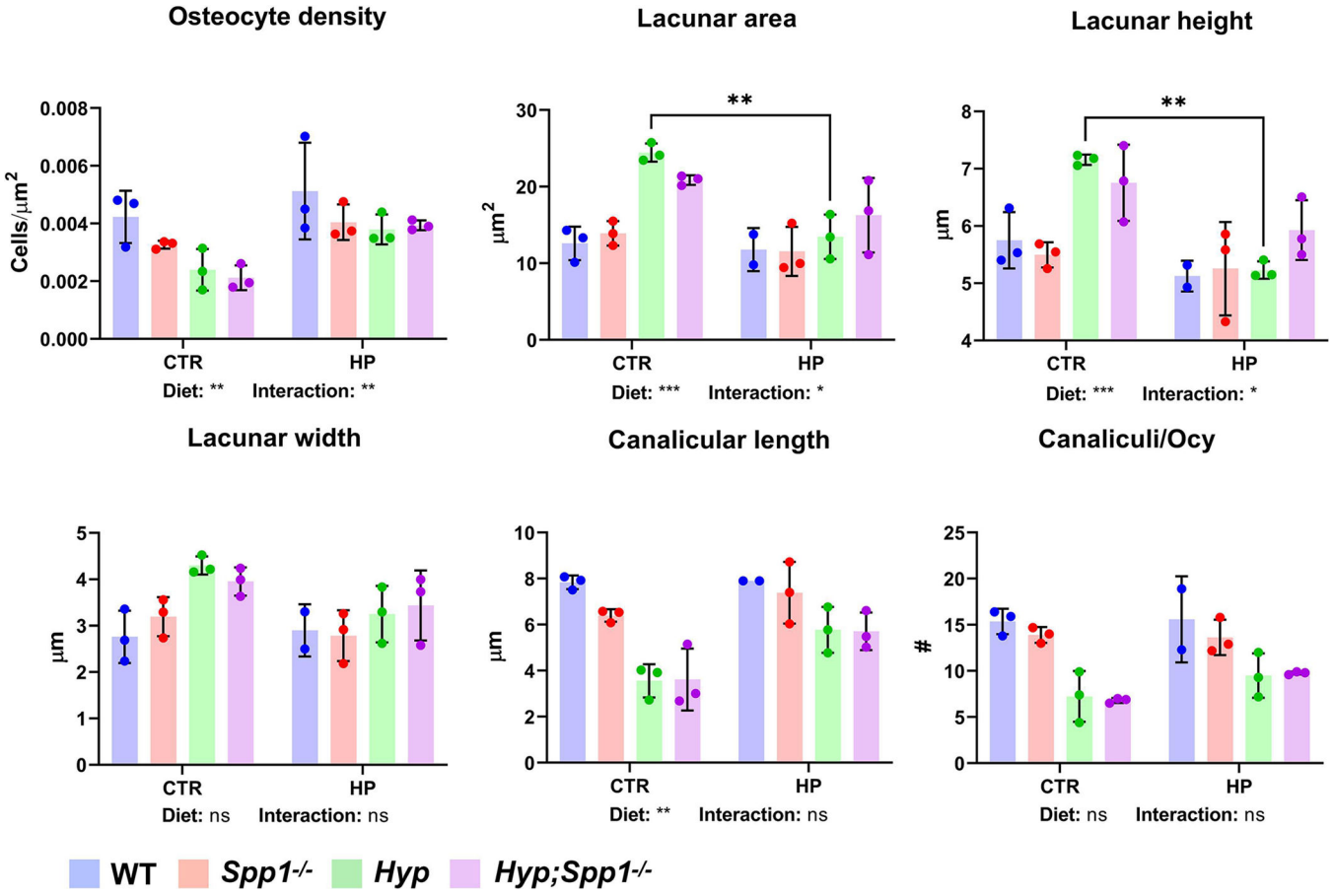

Fig. 8. Genotype-diet interactions in improved osteocyte lacunocanalicular properties of *Hyp* and *Hyp*;*Spp1*$^{-/-}$ mice.

Comparisons across diet (CTR vs. HP) are shown between mice of the same genotype. Comparisons between genotypes are shown in Figures 3 and 7. Two-way ANOVA with post-hoc Tukey test indicated statistically significant genotype-diet interactions in CTR vs. HP diets. *P*-values are shown for both diet and interactions beneath each graph. ** $P<0.01$.